Multiscale defect cluster excitations in the melting transitions of two-dimensional Yukawa systems

Yen Chiu, Hao-Wei Hu, Yun-Xuan Zhang, and Lin I*
Department of Physics and Center for Complex Systems, National Central University, Jhongli, Taoyuan City 32001, Taiwan

(Received 13 September 2023; accepted 13 February 2024; published 15 March 2024)

In this work, we numerically demonstrate and classify the intermittently emerged multiscale defect clusters (DCs) composed of few to tens of disclinations, in the two-stage solid-hexatic-liquid melting transition of a two-dimensional Yukawa system. We uncover the topological pathways for their formation and how the crystalline-ordered domains (CODs) with different lattice orientations nearby DCs can be formed, which affect the structural order variations in the transitions. It is found that the six basic processes: the pair generation (I), dissociation (II), scattering (III), propagation (IV), recombination (V), and pair annihilation (VI) of dislocations, each through a single bond-breaking-replacement process, govern DC evolutions. Small DCs composed of antiparallel dislocations through process I by localized particle-shear motion dominate in the solid phase. The further successive combination of processes II to IV, through successive bond-breaking-replacement rotations by stringlike cooperative hopping of several particles, are responsible for the formation of open and ring-shaped stringlike DCs composed of connected dislocations, free dislocations, free disclinations, and CODs enclosed by stringlike DCs, dominated in the hexatic phase. The spreading of neighboring small DCs or the emergence of new small DCs nearby can generate larger DCs with tens of dislocations. The combinations of reversed basic processes can break or diminish a DC. Even though the two-stage transitions can also be signified by the onsets of the rapid rises of the free disclinations and free dislocations successively, the increases of the number and averaged size of multiscale DCs enclosing CODs play the key roles for the successive losses of translational and orientational orders in the two-stage phase transitions.

DOI: 10.1103/PhysRevResearch.6.013288

I. INTRODUCTION

The melting transition of the two-dimensional (2D) system is an intensively studied fundamental physics issue [1–35]. Unlike the single-stage solid-liquid phase transition demonstrated in some systems [30–35], the two-stage defect-mediated second-order transition from the crystalline phase through the intermediated hexatic phase to the liquid phase, has been predicted theoretically [1–4], and demonstrated experimentally and numerically in various 2D systems, mainly with soft interactions [5–29]. Magnetic bubble arrays [5], electrons on liquid surfaces [6], monolayer colloidal suspensions in liquids [7–15], cellular (Pot model) systems [16], skyrmion systems [17], air driven 2D granular systems [18], dusty plasmas [19,20] and Yukawa systems [21–23], are good examples. The well-known Kosterlitz-Thouless-Halperin-Nelson-Young (KTHNY) theory [1–4] suggested that the successive emergences of low-density thermally excited free dislocations (five- and sevenfold disclination pairs) and free disclinations with increasing temperature lead to the loss of the long-range translational order, associated with the slow power-law decay of long-range orientational order in the hexatic phase, followed by the exponential decay of both translation and orientational orders in the liquid phase, respectively. In previous related studies, the translational and bond-orientation orders, the scaling behaviors of their spatial correlation functions, the numbers of free dislocations and free disclinations, and the total number of all defects have been used as common statistical variables to characterize the melting behaviors and identify the different types of melting scenarios [5,7,9–26,28–30,33,35].

In addition to free dislocations and free disclinations, around the melting transition, multiscale defect clusters (DCs) of connected disclinations can be observed in defect configuration plots of many previous works for various systems exhibiting two-stage KTHNY transition [5,7,9–11,13–17,19–24,26–29] or first-order transition [30,33]. Some of the small DCs were classified [26,29]. Open- and closed-loop stringlike hoppings leading to the formations of interstitial-vacancy defect pairs and small ringlike DCs, respectively, were also demonstrated [27,36]. Although without specifically pointing out, crystalline-ordered domains (CODs) with different lattice orientations surrounded by DCs (mainly stringlike DCs) can be observed in particle images of many previous papers [11,19,21,24,28–30,33]. Nevertheless, beyond the free dislocation and free disclination picture of the KTHNY theory and the limited studies of measuring the size distributions of DCs under different temperatures for the two-stage melting transition [23], the following issues remain unexplored: (i) the kinetic pathways for the formations and fluctuations of different classes of multiscale DCs, and consequently the formations and fluctuations of enclosed CODs, and (ii) why

*lini@phy.ncu.edu.tw

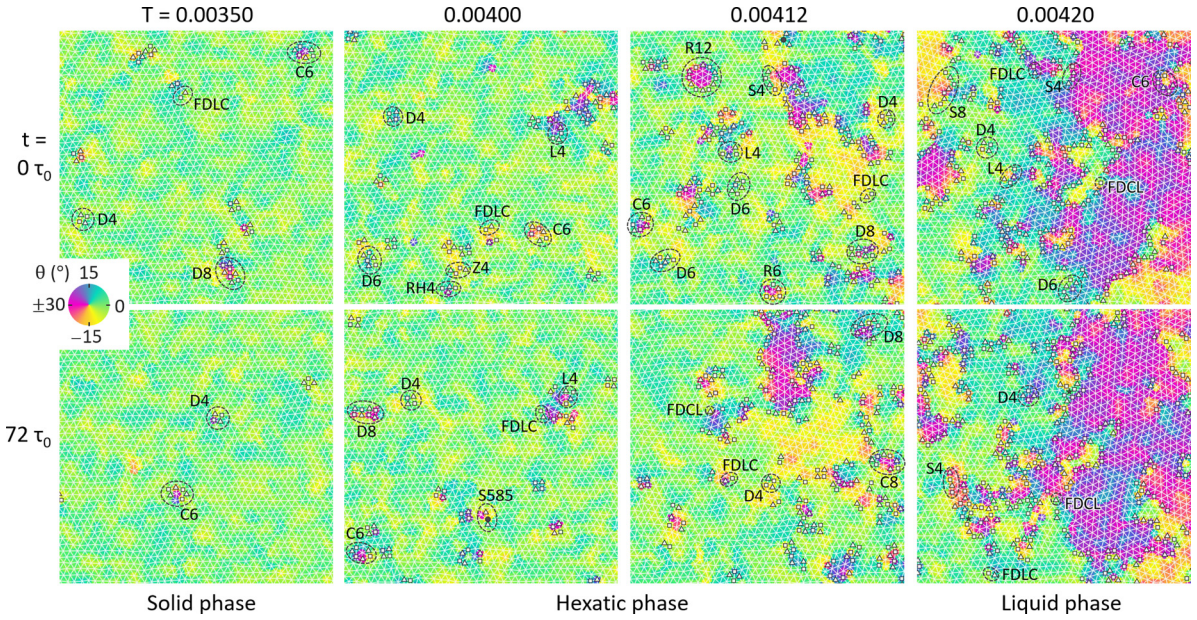

FIG. 1. Particle configurations (particles are located at the vertices of the background grid, with fivefold and sevenfold disclination defects represented by triangles and squares), color coded by θ, at different times for the solid phase, the two hexatic phases, and the liquid phase at $T = 0.00350$, 0.00400, 0.00412, and 0.00420, respectively. Different types of DCs are classified and labeled.

the slow decay of orientational order is still sustained in the hexatic phase.

Microscopically, for a 2D triangular lattice, defects are the sites with nearest-neighbor number deviating from 6 [37–40]. The accumulation of sufficient stochastic thermal or external stress perturbations can generate stick-slip hopping in the form of string or vortices [27,36,41–49]. The induced shear motions of adjacent particles cause topological rearrangement through bond-breaking reconnection, and affects defect dynamics [27,36,41,43,44,46–50]. However, the past works on defect dynamics in 2D melting and cold liquids have mainly focused on free dislocations, the generation of the small DC formed by a pair of antiparallel dislocations, interstitial and vacancy defects in equilibrium and nonequilibrium 2D solids or cold liquids [13–15,27,36,41,43,46–50]; and the diminishing stringlike DCs in the relaxation of deeply quenched liquids [44].

In essence, in the 2D melting transition, the increasing thermal agitation can enhance stringlike cooperative hopping and consequently different types of structural rearrangement for generating free dislocations or even multiscale DCs from the ordered triangular lattice. It could consequently affect COD formation and the loss of structural order. Certainly, it is important to construct a clear physical picture to further unravel the following unexplored issues for the two-stage melting transitions: (i) more detailed classification of different types of multiscale DCs, and the corresponding basic topological pathways governing the excitations and evolutions of different types of DCs from free disclinations to large DCs, (ii) how CODs with different lattice orientations are generated associated with the formation of multiscale DCs around their interfaces through cooperative particle hopping, and (iii) the roles of the fluctuating multiscale DCs and CODs on the structural order changes, beyond the KTNHY picture based on the increasing free dislocation and free disclination unbinding.

In this work, the above unexplored issues are investigated through molecular dynamics simulation for a 2D Yukawa system. We demonstrate and classify the intermittently emerging and fluctuating multiscale DCs up to tens of connected seven- and fivefold disclinations with increasing averaged DC size in the two-stage solid-hexatic-liquid melting transition. In addition to the conventional statistical measures of spatial correlations functions of particle position and bond-orientation order, and defect number at different temperatures for evidencing the two-stage melting transition [5,7,9–26,29], the above unexplored issues are uncovered through monitoring and correlating the spatiotemporal evolutions of: (i) DC and COD fluctuations, (ii) local bond-breaking replacements and lattice orientation fluctuations, and (iii) cooperative particle motion causing bond-breaking replacement and structural rearrangement, under different temperatures.

II. NUMERICAL METHOD

The molecular dynamic simulation using 16 384 particles in a rectangular box with periodic boundary condition is conducted, using large-scale atomic/molecular massively parallel simulator (LAMMPS) [51]. The box aspect ratio is $2/\sqrt{3}$, allowing the loading of the perfect triangular lattice at zero temperature. The coupled Langevin equation of motion of particle i with mass m follows: $m\ddot{x}_i = -\sum_{j\neq i}^{N} \nabla U_{ij} - \nu m\dot{x}_i + \zeta$, where U_{ij}, ν, and ζ are the interacting potential of particle pair i and j, friction coefficient, and spatially and temporally uncorrelated thermal (Gaussian) noise, respectively. $\zeta^2/m\nu$ is the effective temperature T. $U_{ij} = \frac{Q^2 e^{-r_{ij}/\lambda_D}}{4\pi\epsilon_0 r_{ij}}$ is the Yukawa potential for particle pair with separation r_{ij}, where Q, λ_D, and ϵ are the particle charge, Debye length, and electric permittivity, respectively. The screening parameter $\kappa = r_w/\lambda_D$ and the damping rate ν/ω_0 are fixed at 0.4 and 0.14,

respectively, where r_w is the Wigner-Seitz radius and ω_0 is the one-component plasma frequency. The Yukawa potential is truncated at $r_{ij} = 8r_w$. The time unit is $\tau_0 = 1/\omega_0 = (Q^2/2\pi\epsilon_0 ma^3)^{-1/2}$. The time step for integration is 0.01 τ_0.

III. RESULTS AND DISCUSSION

A. Multiscale defects at different temperatures

Figure 1 shows typical particle configurations at different times and different temperatures T, where particles are located at the vertices of the background grids and the time unit τ_0 is the inverse of the one-component plasma frequency. Squares and triangles represent seven- and fivefold disclination defects, respectively. The local orientational order $\Psi_6(\mathbf{r}) = |\Psi_6|e^{i6\theta} = \frac{1}{N}\sum_i e^{i6\theta_i}$ for the particle at $\mathbf{r}$ is measured, where N and θ_i are the number of its nearest neighbors, and the angle of the bond from it to its nearest neighbor i, respectively [39]. Figure 1 is color coded by θ, the phase of $\Psi_6(\mathbf{r})$.

Figure 2(a) shows g_{tr} and g_{6r}, the spatial correlation function of Ψ_t and Ψ_6, versus r/a at different T, where $\Psi_t(\mathbf{r}) = e^{i\mathbf{G}\cdot\mathbf{r}}$ is the local translational order, $\mathbf{G}$ is the primary reciprocal lattice vector, and a is the mean lattice constant. Figure 2(b) shows the change of the scaling exponents α of g_{tr} and β of g_{6r} with increasing temperature T. Figures 2(a) and 2(b) manifest the earlier deterioration of the translational order than the orientational order with increasing temperature. Same as those in the colloidal system studies [13,14,21], the temperatures for scaling exponents α and β reaching $-1/3$ and $-1/4$ are used to identify the temperatures for the solid-hexatic and the hexatic-liquid transitions, respectively. The system enters the hexatic phase at $T = 0.00388$ with power-law decays of g_{6r}, and changes to the liquid phase at $T = 0.00414$, where g_{6r} starts to show exponential decay [Fig. 2(a)].

As shown in the panels at different times in Fig. 1 (also see Fig. S1 [52] for more details), multiscale DCs intermittently emerge and diminish spatiotemporally in the hexatic phases at $T = 0.00400$ and 0.00412, in contrast to the few DCs dominated by dislocation pairs in the solid phase at $T = 0.0035$. Figure 2(c) shows F_n, the averaged number of DCs with size n (the number of connected disclinations in a DC) in a frame, normalized by 16 384 particles at different T. The sawtooth-type curves demonstrate that DCs with 1 to a few connected dislocations (i.e., even number of disclinations) dominate, followed by a rapidly descending tail with n up to a few tens. Increasing T from 0.00400 to 0.00412 increases the total number of DCs, associated with the increasing number of small DCs, the decreasing sawtooth heights (i.e., the ratio of F_{2i} to F_{2i-1}), and the further expansion of the descending tail of F_n contributed by large DCs. Note that the previous study for the two-stage melting transition of 2D Yukawa systems at $\kappa = 2$ and 4 also demonstrated the similar behaviors of the DC size histograms [23].

B. Topological pathways for defect cluster excitations

Let us focus on classifying small DCs with n about or less than 10 and identifying their formation pathways. As indicated by the examples in Figs. 1 and S1 [52], in addition

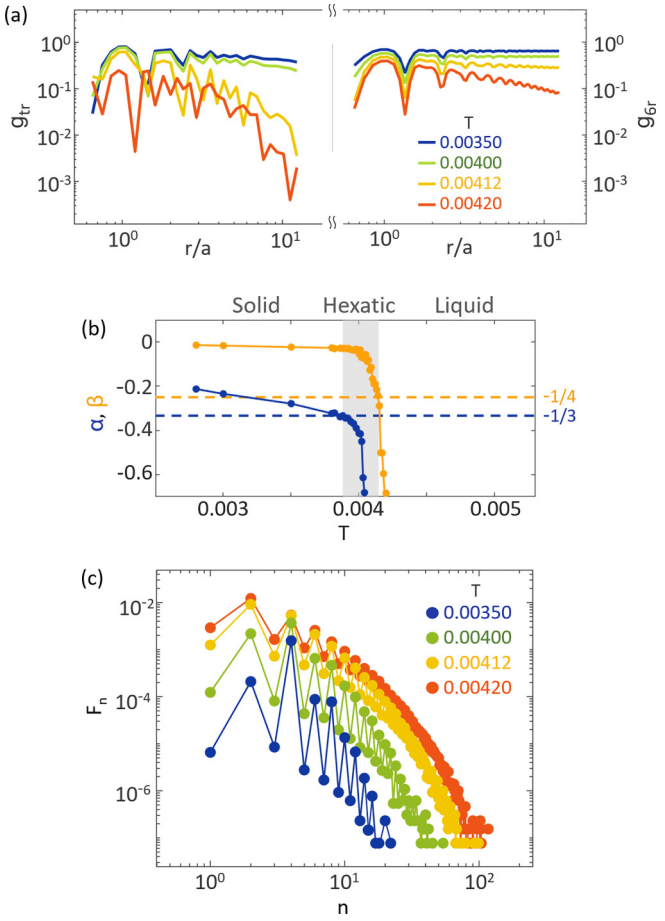

FIG. 2. (a) g_{tr} and g_{6r}, the spatial correlations function of Ψ_t and Ψ_6, respectively, versus r/a at different T, where a is the mean lattice constant. (b) Scaling exponents α and β of g_{tr} and g_{6r}, respectively, versus T. The solid-hexatic and the hexatic-liquid transitions occur at $T = 0.00388$ and 0.00414, as α and β reach $-1/3$ and $-1/4$, respectively. (c) F_n, the average number of DCs with size n (the number of connected disclinations in a DC) in a frame, normalized by the total number of particles (16 384 particles) in a frame at different T.

to free disclinations and free dislocations, small DCs can be roughly classified into: (i) densely packed DCs with square or rectangular shape composed of antiparallel dislocations connected side by side, named as Dn, and (ii) ringlike and open-string DCs, each composed of n alternatively connected seven- and fivefold disclinations in the form of a string. The former is named as Rn. The C-shaped open string with two abrupt turning ends is named as Cn. The L-shaped short string with one abrupt bending end and four disclinations is named as L4. Other open strings are named as Sn.

Under the conservations of Burgers vectors (BVs, the vectors normal to the bonds connecting the pairs of five- and sevenfold disclinations, each with $+\pi/3$ and $-\pi/3$ topological charges, respectively) and the overall topological charges, the following six basic dislocation processes as sketched in Fig. 3(a) and their combinations play the main roles governing dislocation dynamics around melting. They are: (I) pair generation of dislocations with opposite BVs, (II) dissociation of one dislocation into two dislocations with 120° BV angle

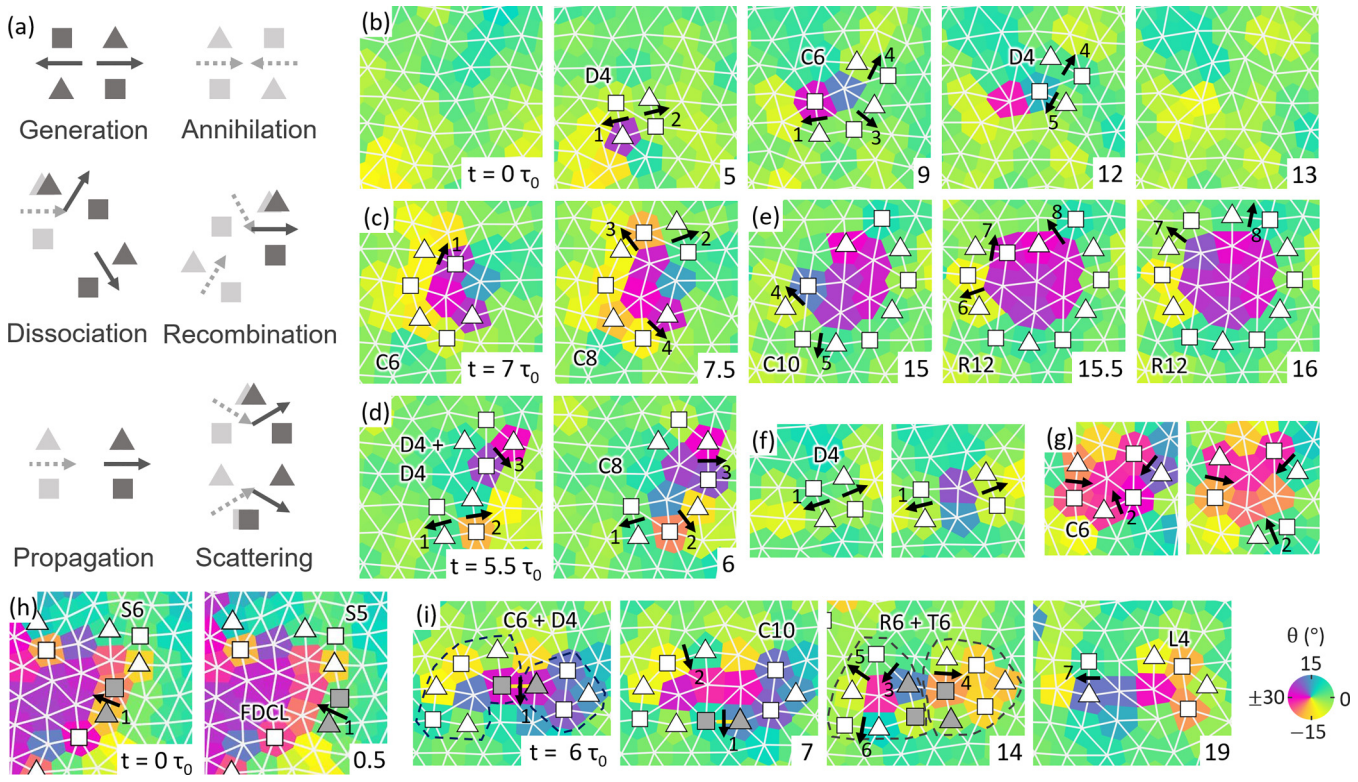

FIG. 3. (a) Sketches for the six basic dislocation processes. The arrows denote the Burgers vectors normal to the bond connecting five- and sevenfold disclinations. The gray and black symbols are used to label the initial and final states of each process, respectively. (b) to (i), examples of the sequential particle and defect configuration images, color coded by θ, showing the typical pathways for generating different types of small DCs.

difference, (III) scattering of two dislocations with 60° BV angle difference to another two dislocations with 60° BV angle difference, (IV) propagation of the dislocation along its BV, and (V) and (VI) pair annihilation and recombination of dislocations, the reversed processes of I and II, for reducing dislocation number by two and one, respectively. In Fig. 3(a), the gray (black) symbols are for the initial (final) configurations. Note that, since the dislocation can propagate along or against its BV direction, the above six processes also occur if all the BV directions in each process are reversed.

Figures 3(b) to 3(h) show examples of some commonly occurring kinetic processes for small DCs with n about or smaller than 10. In Fig. 3(b), after the pair generation of dislocations from the defect-free region to form a D4, dislocation 2 dissociates to dislocations 3 and 4 and forms a C6. Then a new D4 with different position and orientation is formed after the recombination of dislocations 1 and 3 to form dislocation 5, followed by the pair annihilation to the defect-free state. Figure 3(c) shows that the dissociation of dislocation 1 at one end of the C6 into dislocations 2 and 3 forms a C8. Figure 3(d) shows that the scattering of the dislocations 2 and 3 from the two connected D4s with 60° BV angle difference also forms a C8. Then the dissociation of dislocation 1 at one corner of the C8 of Fig. 3(d) to dislocations 4 and 5 in the first panel of Fig. 3(e) forms a C10. The further dissociation of dislocation 4 to dislocations 6 and 7 forms an R12 with indented upper part, which can move outward to around the R12 through the scattering of dislocations 7 and 8.

Free dislocations (labeled as FDLCs) can be formed by the detachment of a dislocation from a DC through its propagation along or against its BV. Figures 3(f) and 3(g) show two examples of forming two and three free dislocations, after dislocations 1 and 2 move apart from a D4 and a C6, respectively. Figure S3(c) further shows another example of forming three free dislocations with larger separations [52].

Figure 3(h) shows that two neighboring gray disclinations of the stringlike DC composed of three connected dislocations can re-pair to form a dislocation, which propagates against its BV. It generates a free disclination and a stringlike DC (named as S5) with five disclinations. Figure S3(e) shows another example in which the propagation of a newly re-paired dislocation is also responsible for breaking a mother DC with even n to smaller DCs with odd n [52].

We also observe the formation of the interstitial-vacancy pair. Figure 3(i) shows that the two neighboring seven- and fivefold disclinations from the two connected C6 and D4 can form the new dislocation 1 and propagate downward. It leads to the formation of a C10 at $t = 7\ t_0$, followed by the dissociation of dislocation 2 into dislocation 3 and dislocation 4, and the formation of a DC composed of a ring-shaped DC (R6) and a triangular-shaped DC (T6), each formed by three connected dislocations at $t = 14\ t_0$. The R6 has an extra particle at the center, in contrast to the T6 whose three sevenfold disclinations are connected with each other. Namely, the centers of R6 and T6 correspond to the interstitial and the vacancy points, respectively [27,36]. The recombination of dislocation 5 and 6 to dislocation 7 and the pair annihilation

of the two gray dislocations at $t = 14\ \tau$ in Fig. 3(i) leads to a free dislocation and an L-shape DC (L4) at $t = 19\ \tau_0$.

In Figs. S3(a) and S3(b) [52], we also show examples of the topological pathways for the formations of vacancies and interstitials at the centers of small DCs with other shapes. All the above DCs with interstitial or vacancy, and small DCs such as L4 and C6, have been reported in the previous studies for the hexatic phase but without addressing their topological formation pathways [27,36].

In brief, under the conservation of BVs, the six basic processes I to VI shown in Fig. 3(a) and the higher-order processes through their different successive combinations lead to the formation and evolution of different types of small DCs described in Fig. 3. The pair generation of dislocations is responsible for the formation of the Dn. The successive dissociations and scattering of dislocations are responsible for turning a single D4 into a curved stringlike DC. The detachments of dislocations through propagation along their BVs from mother DCs lead to the free dislocation and free disclination formations. Interstitial and vacancy DCs are generated through the complicated combination of the above six processes. Small DCs could diminish through reversed processes after their sporadic emergences. Note that the above six processes were also demonstrated as the keys governing the DC dynamics in the cold 2D dusty plasma liquid, and the relaxation of a quenched 2D Yukawa liquid to solid exhibiting diminishing DCs (mainly stringlike DCs) [41,44]. Pair generation of propagating free dislocations from a D4 was also reported in 2D dusty plasma crystal [49].

As shown in the two sets of sequential images of Figs. 4(a) and 4(b) in two different regions of the hexatic phase, large DCs mainly composed of connected small dense DCs and stringlike DCs, can also be formed through the coalescence of small unconnected DCs after their spreading, and/or the emergence of other defects between them. After that the large DC can change its shape and size, or break into smaller DCs, which can partially resume the lattice orientation in the region occupied by the large DC. It is the key for sustaining the slow decay of the temporal correlation function $g_{6\tau}$ of Ψ_6 in Fig. 4(c).

Note that, in a defect-free region, the six basic processes in Fig. 3(a) mainly generated DCs composed of connected dislocations, i.e., DCs with even number of disclinations, mainly in the form of antiparallel dislocations connected side by side or strings of dislocations connected head to tail. The additional process of breaking a mother DC with even number of disclinations into smaller DCs with odd number of disclinations (including the free disclination) is more complicated and is harder to occur in the low-temperature regime. It leads to the large tooth height of the sawtooth pattern of F_n (i.e., the ratio of F_{2i} to F_{2i-1}, where i is an integer), which can be decreased by increasing temperature, as shown in Fig. 2(c).

C. Shear-induced bond-breaking replacements for DC excitations

The DC excitation is through the cooperative hopping-induced structural (topological) rearrangement. It is found that each of the six basic processes of dislocations sketched in Fig. 3(a) is achieved through the stretching, breaking, and

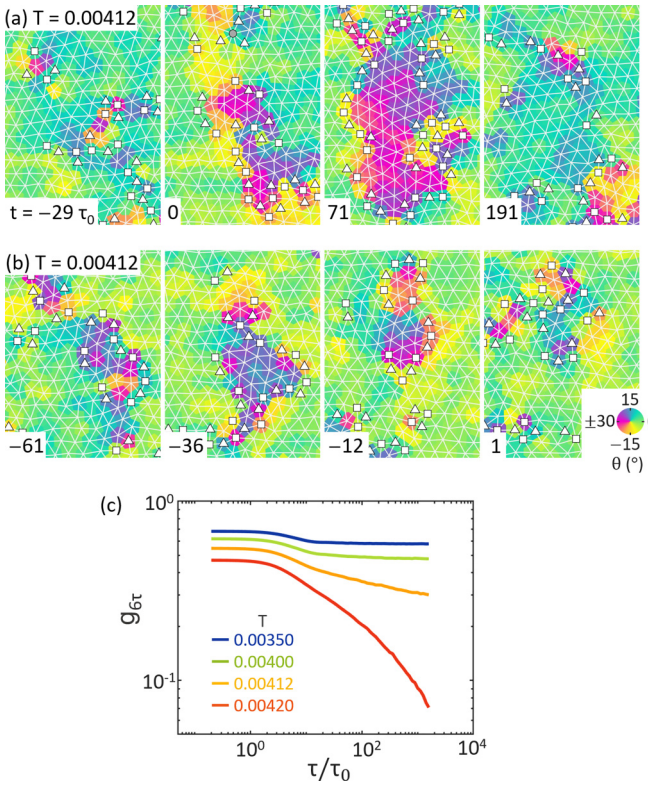

FIG. 4. (a) and (b) Two sets of sequential images in two different regions of the hexatic phase at $T = 0.00412$, showing the excitation and de-excitation of larger DCs through spreading small DCs or emerging new small DCs nearby. The large DC can also break into small DCs and partially diminish to resume the local structural order. (c) Temporal correlation functions $g_{6\tau}$ of Ψ_6 at a few typical temperatures.

replacement of an old bond by a new bond transverse to it, caused by thermally induced shear. In the examples of Fig. 5, in addition to the similar plots of DC evolution, we further add future particle trajectories over time interval Δt, on the initial particle configuration plots at different t, for some of the few basic topological processes of defect evolutions. In each image, each red dotted line labels the bond to be replaced by a new bond transverse to it in the next image, through shear-induced topological rearrangement.

For example, the first trajectory plot of Fig. 5(a) shows that the cooperative left-downward motions of particles C and D, and the upward motion of particle A, can increase the distance between particles A and C and decrease the distance between particles D and B. It causes the replacement of the bond A-C by the new bond B-D, and in turn the generation of the D4 cluster at $t = 5\ \tau_0$ in the second panel. The second trajectory plot further demonstrates that from $t = 0$ to 7.5 τ_0, clockwise cooperative motion of particles F, H, and I, the left-downward cooperative motion of particles G, D, and C, and the rightward motion of particle E, can further replace the bond D-F by bond E-G (see the second to the third panels). It causes the dissociation of the dislocation 1 to dislocations 3 and 4 and the formation of a C6 at $t = 7\ \tau_0$; followed by the dissociation of dislocation 4 to two new dislocations 5 and 6

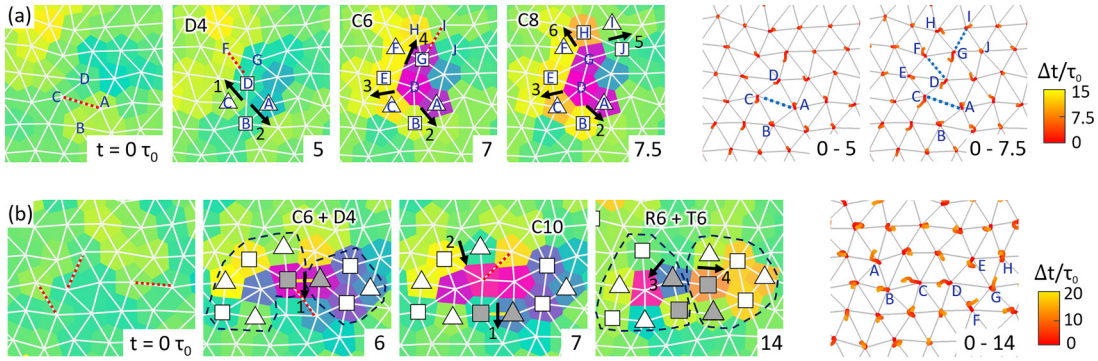

FIG. 5. (a) Left four panels: sequential particle and defect configuration images, color coded by θ, for the generation of a D4, a C6, and a C8. In each image, each dotted line labels the bond to be replaced by a new bond transverse to it in the next image, through shear-induced topological rearrangement. Right two panels: particle configurations at $t = 0\ \tau_0$, with the subsequent particle trajectories over time interval $\Delta t = 5$ and $7.5\ \tau_0$, respectively. Each blue dotted line corresponds to the bond to be replaced by a new bond transverse to it in Δt through relative shear motion. (b) Similar plotting to those of (a) showing how the cooperative leftward (clockwise) motions of particles A, B, C, D, and E, and the upward cooperative motion of particles F, G, and H, can lead to the pair generation of an interstitial and a vacancy at the centers of the R6 and the T6, respectively.

and the formation of C8 at $t = 7.5\ \tau_0$, through the replacement of bond G-I by bond H-J.

Figure 5(b) shows another example for the shear-induced bond-breaking replacement for interstitial-vacancy generation shown in Fig. 3(i). Initially, a DC composed of a C6 connected with a D4 can be formed by breaking the three bonds in the first panel and replacing them by three new bonds transverse to them. Then the gray disclinations from the D4 and the C6, respectively, re-pair to form a new dislocation 1 and move downward through breaking replacement of the dotted bond in the second panel. It generates a new C10. The subsequent dissociation of dislocation 2 to dislocations 3 and 4 by the breaking replacement of the dotted bond in the third panel of Fig. S2(c) [52] forms the R6 connected with T6 in the fourth panel.

The particle trajectory plot in Fig. 5(b) shows that the process of interstitial-vacancy generation is associated with the two separated hopping strings. The clockwise stringlike cooperative motion of particles A to E and the counterclockwise cooperative motion of particles F, G, and H, can make the region around particle A overdense and the region surrounded by particles E, D, F, and G underdense, which generate an interstitial and a vacancy in the above two regions (the centers of the R6 and the T6), respectively.

Figures S2 and S3 [52] show more examples of DC formation and evolution through successive single bond-breaking-replacement events.

D. Correlating structural order variations and multiscale defect excitations

What are the statistical behaviors of important order and disorder (defect) parameters with increasing temperature from the solid state to the liquid state? The top panel of Fig. 6 shows the changes of global translational and orientational orders $|\langle\Psi_t\rangle|$ and $|\langle\Psi_6\rangle|$ with T, where the averages are taken over all particles in the simulation box and total time interval $10^5\ \tau_0$. The middle panel of Fig. 6 shows the averaged numbers of different types of DCs versus T in one frame, where $F_{\rm FDCL}$, $F_{\rm FDLC}$, F_{D4}, $F_{\rm other}$ are the averaged numbers of free disclinations, free dislocations, D4s, and other DCs different from the above DCs, respectively, normalized by the total particle number in each frame. The bottom panel of Fig. 6 shows $N_{\rm FDCL}$ $(= F_{\rm FDCL})$, $N_{\rm FDLC}$ $(= 2F_{\rm FDLC})$, N_{D4} $(= 4F_{D4})$, and $N_{\rm other}$ versus T, corresponding to the averaged numbers of all disclinations in all free disclinations, all free dislocations, all D4s, and all other DCs different from the above DCs in a frame, respectively, normalized by the total particle number in each frame. Note that one thousand frames with $100\ \tau_0$ sampling intervals are used for the statistics. The inset shows the blown-up curves around the transition region of the bottom panel of Fig. 6.

Now we construct a physical picture for understanding the change of translational and orientational orders in the melting transition from the view of multiscale defect excitations. Note that, as shown in Figs. 5, S2, and S3 [52], the shear-type relative motion of two neighboring particles can easily rotate and extend the bond connecting them and cause the stretching-breaking of that bond and the replacement by a new bond transverse to it. Each of the six basic dislocation processes is achieved by a single bond-replacement event. It takes: (A) a single bond-breaking replacement by localized shear for forming a D4 through process I (pair generation), and (B) further successive bond-breaking-replacement steps for different combinations of processes I to VI of dislocations through the successive hopping of particles in the cooperative hopping string, and the formation of other types of DCs.

The four sets of plots of sequential particle trajectories over $40\ \tau_0$ interval, color coded by $\Delta r/a$ (Δr is the particle displacement over $40\ \tau_0$ and a is the mean lattice constant) in Fig. 7, illustrate cooperative motions at different temperatures. In the solid phase, the low temperature mainly allows more localized shear excitation (see Fig. 7). Process A and its reverse process thereby dominate. It allows easier excitation and de-excitation of the D4, a quadrupole composed of disclinations with $+\pi/3$ and $-\pi/3$ topological charges (note that F_{D4} starts to rise at $T = 0.0028$). It causes 50 times higher probability of D4s than other DCs in the solid phase at $T = 0.00350$, as

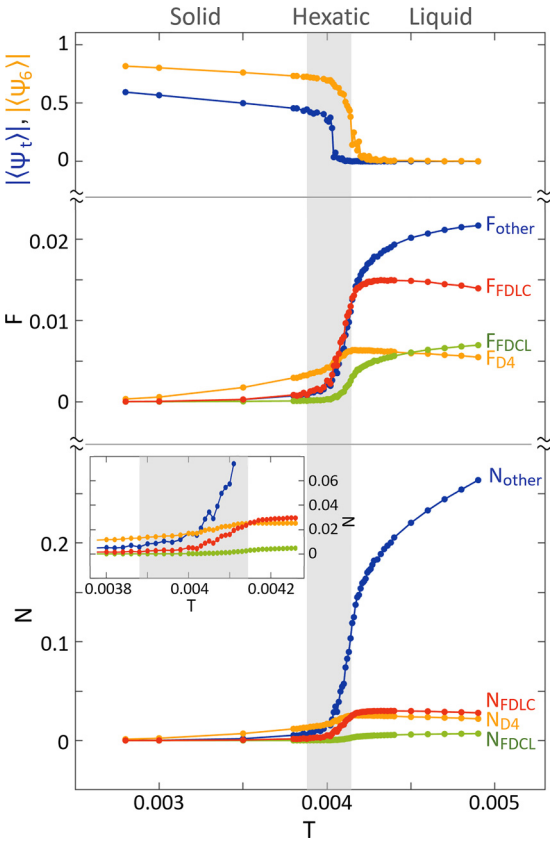

FIG. 6. Top panel: $|\langle\Psi_6\rangle|$, and $|\langle\Psi_t\rangle|$ versus T, where the averages are taken over all particle sites in the simulation box and total time interval 10^5 τ_0. Middle panel: averaged numbers of different types of DCs versus T in a frame, where $F_{\rm FDCL}$, $F_{\rm FDLC}$, F_{D4}, and $F_{\rm other}$ are the averaged numbers of free disclinations, free dislocations, D4s, and other DCs different from the above DCs, respectively. Bottom panel: $N_{\rm FDCL}$ $(= F_{\rm FDCL})$, $N_{\rm FDLC}$ $(= 2F_{\rm FDLC})$, N_{D4} $(= 4F_{D4})$, and $N_{\rm other}$ versus T, corresponding to the averaged numbers of all free disclinations; and disclinations in all free dislocations, all D4s, and all other DCs different from the above DCs in a frame, respectively. The inset shows the blown-up curves around the transition region. Note that each data is normalized by the total particle number in a frame. One thousand frames with 100 τ_0 sampling intervals are used for the statistics.

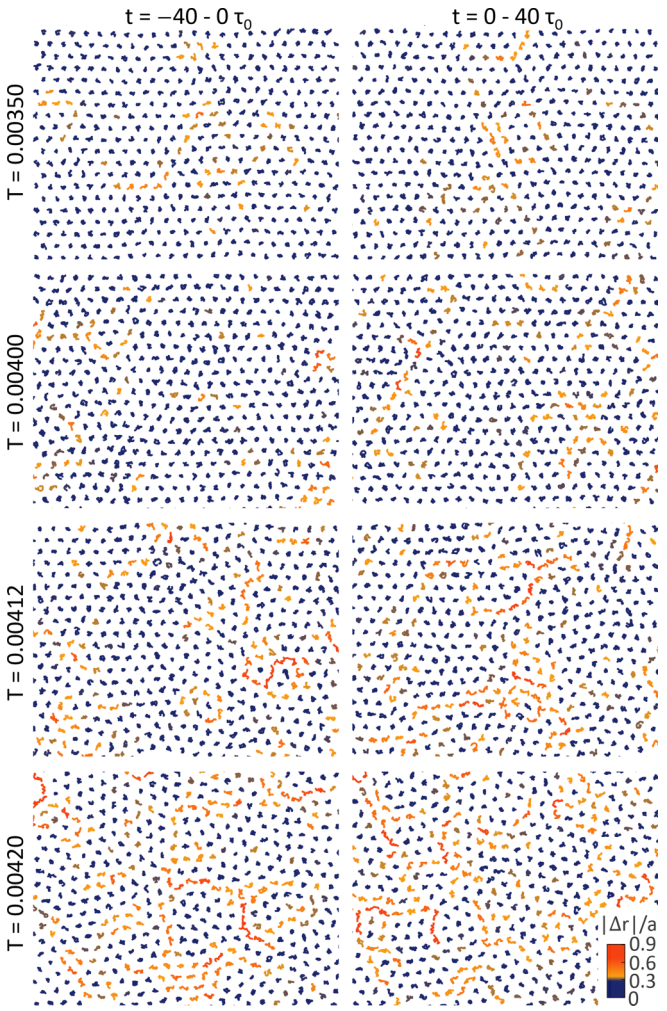

FIG. 7. Four sets of sequential plots of particle trajectories over 40 τ_0 interval (middle and bottom row), color coded by particle displacement $\delta r/a$ (a is the mean lattice constant) over 40 τ_0, at $T = 0.00350$, 0.00400, 0.00412, and 0.00420.

shown in Fig. 2(c). This can also be evidenced by the growth of the DC cluster number dominated by the growth of F_{D4} (D4 number) with increasing T shown in Fig. 6. The small contribution by the growth of $F_{\rm other}$ is mainly by C6 with three connected dislocations, D8 and D12 with two and three connected D4s, respectively, or D2, D6, and D10 by detaching one dislocation from D4, D8, and D12, respectively. Note that, because of their extremely low emergence probabilities, not all of them appear in Figs. 1 and S1 [52].

The shear motion and bond-breaking replacement also cause bond rotations and change θ (local bond orientation, e.g., see the orange and purple regions in Figs. 3, 4, S2, and S3 [52]). The D4 and other Dn are only associated with highly localized change of θ in or around them induced by the localized shear. With increasing T in the solid phase, the increasing fractions of D4 and other Dn only slowly decrease $|\langle\Psi_t\rangle|$ and $|\langle\Psi_6\rangle|$, as shown in Fig. 6.

Further increasing temperature allows the excitations of longer cooperative hopping strings with several particles (see Fig. 7), and consequently the higher probability for process B to turn dense DCs mainly into C- and ring-shape small DCs, and free dislocations detached from the above DCs. Some larger DC can also be sporadically excited. It leads to the larger increase rates of $F_{\rm FDLC}$, $F_{\rm other}$, $N_{\rm FDLC}$, and $N_{\rm other}$, which cause the onset of the rapid loss of the translational order, evidenced by the onsets of the rapid drop of α and $|\langle\Psi_t\rangle|$ at the solid-hexatic phase transition.

The successive topological processes dominated in the hexatic phase cause θ changes in the regions enclosed by C- and ring-shaped small DCs, or the curved stringlike large DCs composed of disclinations up to a few tens. It induces the sporadic formation of CODs with lattice orientations different from the background lattice which sustains the long-range orientational order. The COD disappearance can resume the local lattice orientational order. Namely, the spatiotemporally intermittent emergence and disappearance of DCs in the hexatic phase only causes the slow decays of g_{6r} in Fig. 2(a) and

$g_{6\tau}$ in Fig. 4(c), with increasing r and τ, respectively, in the first half-temperature regime of the hexatic phase.

Further increasing T leads to the rapid rises of $F_{\rm FDLC}$, $F_{\rm other}$, $N_{\rm FDLC}$, and $N_{\rm other}$, and the transition to the liquid phase, shown in the middle panel of Fig. 6. In the liquid phase, the higher temperature facilitates larger-scale and more frequent cooperative hopping (Fig. 7). It induces more complicated combinations of topological processes I to VI for forming many larger CODs separated by long dislocation strings to accommodate the different lattice orientations (Fig. 1). The large CODs can further split to smaller CODs or coalesce to form larger CODs with different orientations (Figs. 4 and S1 [52]). It is hard to reverse all the complicated sequential processes one by one and thereby causes the losses of the spatiotemporal orientational memory and in turn the fast decay of g_{6r} and $g_{6\tau}$ with increasing r and τ, as shown in Figs. 2(a) and 4(c), respectively, and the rapid drop of $|\langle\Psi_6\rangle|$ to zero with increasing T shown in the top panel of Fig. 6.

The increasing temperature from the hexatic phase to the liquid phase also facilitates the breaking of a mother DC composed of dislocations (i.e., DC composed of even number of disclinations) to two separated DCs each with odd number of disclinations (see the examples of Figs. 3(h), S3(d), and S3(e) [52]). It leads to the rapid rise of free-disclination fraction around the hexatic-liquid transition. Intuitively, a single fivefold (sevenfold) disclination strongly bends the lattice lines toward (away) it and strongly deteriorates the long range structural order correlation [37–40]. However, in our melting transition, a free disclination sporadically detached from a mother DC is achieved through a single bond-breaking replacement which only slightly changes the surrounding local orientational order (see the very small changes of colored (coded by θ) patterns in the sequential images of Fig. 3(h) and S3(d) [52]). It thereby has a much smaller contribution on the deterioration of long range structural order than its mother DC, other abundant multiscale DCs, and their nearby CODs.

According to the KTHNY theory [1–4], the rapid rises of free dislocations and free disclinations, unbinding from other DCs, lead to the solid-hexatic and the hexatic-liquid transitions, respectively. Our findings indeed show that the increasing rates of $F_{\rm FDLC}$ and $F_{\rm other}$ both start to increase around the solid-hexatic transition, followed by their rapid rises at the hexatic-liquid transition. $F_{\rm FDCL}$ also starts to increase in the second half-temperature regime of the hexatic phase and exhibits a high increase rate at the hexatic-liquid phase transition. However, $N_{\rm other}$ is much larger than $N_{\rm FDLC}$ and $N_{\rm FDCL}$ in the two transitions. A single other type DC not only has low $|\Psi_t|$ and $|\Psi_6|$ at their constituting disclination sites but also induces a nearby COD with different orientations for reducing translational and orientational orders, and spatial order correlations.

Namely, the two transitions can both be signified by the onsets of the rises of the numbers of free dislocations and free disclinations, respectively (see Fig. 6). Nevertheless, the onset of the rise and the steepest rise of the fraction of multiscale DCs dominated by abundant amount of connected dislocations are predominantly responsible for the successive deteriorations of translation order and orientational order for the two transitions, respectively.

IV. CONCLUSION

In conclusion, we have numerically demonstrated the spontaneous excitations of multiscale DCs, dominated by a large fraction of small DCs composed of a few dislocations and a small fraction of large DCs composed of disclinations up to a few tens, in the two-stage melting transitions of a 2D Yukawa system. Different types of DCs are classified. The kinetic pathways for their formation and fluctuations, the origins for forming multiscale CODs surrounded by stringlike DCs, and their effects on the spatiotemporal variations of structural orders in melting transitions are unraveled. The major new findings are listed below.

(i) DCs can be classified into: (a) dense DCs with antiparallel dislocations, (b) stringlike DCs each composed of disclinations with alternating topological charges, and (c) large DCs composed of the above two types of DCs. The stringlike DCs can be further classified into ringlike, short-sticklike, C-shape, L-shape, and other weakly curved stringlike DCs. The small interstitial and vacancy DCs are also observed. Under BV and topological charge conservations, the combination of the following six basic processes: (I) pair generation, (II) dissociation, (III) scattering, (IV) propagation, (V) recombination, and (VI) pair annihilation of dislocations, each caused by the shear-motion-induced single bond-breaking-replacement event, mainly govern the formation and evolution of DCs from free disclination to DCs with n up to a few tens.

(ii) In the solid phase, process (I) through thermally induced local shear is responsible for generating dense DCs dominated by D4s and D8s. In the hexatic phase, the higher temperature allows stronger stringlike cooperative hopping involving a few particles for causing successive bond-breaking replacements. It is responsible for the generation of L-, C-, and ring-shaped small stringlike DCs with around or less than 10 disclinations, free disclinations, free dislocations, interstitials, and vacancies, mainly through different combinations of processes (II) to (IV). Reversed processes also occur for diminishing a small DC. The spreading and/or the emergence of nearby small DCs can generate a large DC composed of tens of stringlike disclinations. In the liquid phase, the enhanced hopping with increasing temperature leads to the more complicated successive topological processes for the generation of more DCs with larger size. The temporary detachment of free disclinations from mother DCs leaves daughter DCs with odd number of connected disclinations.

(iii) The successive shears and bond-breaking replacements in the DC formation can cause bond rotations, and the formation of CODs enclosed by stringlike DCs for accommodating the different lattice orientation from background lattice orientation.

(iv) In the hexatic phase, the sporadic emergence and disappearance of multiscale DCs and nearby CODs only intermittently change the local lattice orientation from the background ordered lattice. It is the key for the slow spatiotemporal power-law decays of orientational order. However, in the cold liquid phase, the complicated successive topological processes through complicated cooperative hopping are hard to reverse, which lead to the steep rise of multiscale DC numbers and the rapid loss of the spatiotemporal

orientational memory. The increases of the number and averaged size of multiscale DCs enclosing CODs with different lattice orientations play the key roles for the successive losses of translational and orientational orders in the two-stage phase transitions, even though the transitions can be signified by the onsets of the rapid rises of the free disclinations and free dislocations successively.

This study sheds light on and opens new studies for understanding the generic dynamical behaviors of multiscale DC and associated COD excitations, and their impacts on the structural order variations in the two-stage melting transitions for other different 2D systems with softcore interactions.

ACKNOWLEDGMENT

This work is supported by the Ministry of Science and Technology of Taiwan, under Grant No. MOST-111-2112-M-008-017.

[1] J. Kosterlitz and D. J. Thouless, Ordering, metastability and phase transitions in two-dimensional systems, J. Phys. C **6**, 1181 (1973).

[2] B. I. Halperin and D. R. Nelson, Theory of two-dimensional melting, Phys. Rev. Lett. **41**, 121 (1978).

[3] D. R. Nelson and B. I. Halperin, Dislocation-mediated melting in two dimensions, Phys. Rev. B **19**, 2457 (1979).

[4] A. P. Young, Melting and the vector Coulomb gas in two dimensions, Phys. Rev. B **19**, 1855 (1979).

[5] R. Seshadri and R. M. Westervelt, Statistical mechanics of magnetic bubble arrays. II. Observations of two-dimensional melting, Phys. Rev. B **46**, 5150 (1992).

[6] M. A. Stan and A. J. Dahm, Two-dimensional melting: Electrons on helium, Phys. Rev. B **40**, 8995 (1989).

[7] C. A. Murray and D. H. Van Winkle, Experimental observation of two-stage melting in a classical two-dimensional screened Coulomb system, Phys. Rev. Lett. **58**, 1200 (1987).

[8] C. A. Murray and R. A. Wenk, Microscopic particle motions and topological defects in two-dimensional hexatics and dense fluids, Phys. Rev. Lett. **62**, 1643 (1989).

[9] C. A. Murray, W. O. Sprenger, and R. A. Wenk, Comparison of melting in three and two dimensions: Microscopy of colloidal spheres, Phys. Rev. B **42**, 688 (1990).

[10] R. E. Kushner, J. A. Mann, J. Kerins, and A. J. Dahm, Two-stage melting of a two-dimensional colloidal lattice with dipole interactions, Phys. Rev. Lett. **73**, 3113 (1994).

[11] K. Zahn, R. Lenke, and G. Maret, Two-stage melting of paramagnetic colloidal crystals in two dimensions, Phys. Rev. Lett. **82**, 2721 (1999).

[12] Y. Han, N. Y. Ha, A. M. Alsayed, and A. G. Yodh, Melting of two-dimensional tunable-diameter colloidal crystals, Phys. Rev. E **77**, 041406 (2008).

[13] U. Gasser, C. Eisenmann, G. Maret, and P. Keim, Melting of crystals in two dimensions, ChemPhysChem **11**, 963 (2010).

[14] H. H. von Grünberg, P. Keim, and G. Maret, Phase transitions in two-dimensional colloidal systems, *Soft Matter* (Wiley, New York, 2007), Vol. 3, p. 40.

[15] S. Deutschländer, Melting and spontaneous symmetry breaking in two-dimensional colloidal systems, Ph.D. thesis, Universität Konstanz, Germany (2015).

[16] M. Durand and J. Heu, Thermally driven order-disorder transition in two-dimensional soft cellular systems, Phys. Rev. Lett. **123**, 188001 (2019).

[17] P. Huang, T. Schönenberger, M. Cantoni, L. Heinen, A. Magrez, A. Rosch, F. Carbone, and H. M. Rønnow, Melting of a skyrmion lattice to a skyrmion liquid via a hexatic phase, Nat. Nanotechnol. **15**, 761 (2020).

[18] X. Sun, Y. Li, Y. Ma, and Z. Zhang, Direct observation of melting in a two-dimensional driven granular system, Sci. Rep. **6**, 24056 (2016).

[19] R. A. Quinn and J. Goree, Experimental test of two-dimensional melting through disclination unbinding, Phys. Rev. E **64**, 051404 (2001).

[20] T. E. Sheridan, Monte Carlo study of melting in a finite two-dimensional dusty plasma, Phys. Plasmas **16**, 083705 (2009).

[21] W. K. Qi, Z. Wang, Y. Han, and Y. Chen, Melting in two-dimensional Yukawa systems: A Brownian dynamics simulation, J. Chem. Phys. **133**, 234508 (2010).

[22] A. Radzvilavičius, Geometrical defects in two-dimensional melting of many-particle Yukawa systems, Phys. Rev. E **86**, 051111 (2012).

[23] B. A. Klumov, Two-dimensional Yukawa System: The behavior of defects near the melting region, JETP Lett. **116**, 703 (2022).

[24] Y.-J. Lai and L. I, Defects and particle motions in the nonuniform melting of a two-dimensional Coulomb cluster, Phys. Rev. E **64**, 015601(R) (2001).

[25] S. C. Kapfer and W. Krauth, Two-dimensional melting: From liquid-hexatic coexistence to continuous transitions, Phys. Rev. Lett. **114**, 035702 (2015).

[26] M. Mazars and R. Salazar, Topological defects in the two-dimensional melting, Europhys. Lett. **126**, 56002 (2019).

[27] B. van der Meer, W. Qi, J. Sprakel, L. Filion, and M. Dijkstra, Dynamical heterogeneities and defects in two-dimensional soft colloidal crystals, Soft Matter **11**, 9385 (2015).

[28] W. Qi, A. P. Gantapara, and M. Dijkstra, Two-stage melting induced by dislocations and grain boundaries in monolayers of hard spheres, Soft Matter **10**, 5449 (2014).

[29] P. Digregorio, D. Levis, L. F. Cugliandolo, G. Gonnella, and I. Pagonabarraga, Unified analysis of topological defects in 2D systems of active and passive disks, Soft Matter **18**, 566 (2022).

[30] V. Nosenko, S. K. Zhdanov, A. V. Ivlev, C. A. Knapek, and G. E. Morfill, 2D melting of plasma crystals: Equilibrium and nonequilibrium regimes, Phys. Rev. Lett. **103**, 015001 (2009).

[31] L. Couëdel, V. Nosenko, A. V. Ivlev, S. K. Zhdanov, H. M. Thomas, and G. E. Morfill, Direct observation of mode-coupling instability in two-dimensional plasma crystals, Phys. Rev. Lett. **104**, 195001 (2010).

[32] J. D. Williams, E. Thomas, Jr., L. Couëdel, A. V. Ivlev, S. K. Zhdanov, V. Nosenko, H. M. Thomas, and G. E. Morfill, Kinetics of the melting front in two-dimensional plasma crystals:

Complementary analysis with the particle image and particle tracking velocimetries, Phys. Rev. E **86**, 046401 (2012).
[33] A. V. Ivlev, V. Nosenko, and T. B. Röcker, Equilibrium and non-equilibrium melting of two-dimensional plasma crystals, Contrib. Plasma Phys. **55**, 35 (2015).
[34] S. Maity and G. Arora, Parametric decay induced first-order phase transition in two-dimensional Yukawa crystals, Sci. Rep. **12**, 20430 (2022).
[35] A. Derzsi, A. Z. Kovács, Z. Donkó, and P. Hartmann, On the metastability of the hexatic phase during the melting of two-dimensional charged particle solids, Phys. Plasmas **21**, 023706 (2014).
[36] A. Libál, C. Reichhardt, and C. J. O. Reichhardt, Point-defect dynamics in two-dimensional colloidal crystals, Phys. Rev. E **75**, 011403 (2007).
[37] N. D. Mermin, Rev. Mod. The topological theory of defects in ordered media, Rev. Mod. Phys. **51**, 591 (1979).
[38] J. Weertman and J. R. Weertman, *Elementary Dislocation Theory* (Oxford, New York, 1992).
[39] K. J. Strandburg, *Bond-Orientational Order in Condensed Matter Systems* (Springer, New York, 1992).
[40] P. M. Chaikin, T. C. Lubensky, and T. A. Witten, *Principle of Condensed Matter Physics Vol. 1* (Cambridge University Press, Cambridge, 1995).
[41] C.-H. Chiang and L. I, Cooperative particle motions and dynamical behaviors of free dislocations in strongly coupled quasi-2D dusty plasmas, Phys. Rev. Lett. **77**, 647 (1996).
[42] W.-T. Juan and L. I, Anomalous diffusion in strongly coupled quasi-2D dusty plasmas, Phys. Rev. Lett. **80**, 3073 (1998).
[43] C. Yang, C.-W. Io, and L. I, Cooperative-motion-induced structural evolution in dusty-plasma liquids with microheterogeneity: Rupture, rotation, healing, and growth of ordered domains, Phys. Rev. Lett. **109**, 225003 (2012).
[44] M.-C. Chen, C. Yang, and L. I, Kinetic origin of grain boundary migration, grain coalescence, and defect reduction in the crystallization of quenched two-dimensional Yukawa liquids, Phys. Rev. E **90**, 050401(R) (2014).
[45] C. Yang, W. Wang, and L. I, Avalanche structural rearrangement through cracking-healing in weakly stressed cold dusty plasma liquids, Phys. Rev. E **93**, 013202 (2016).
[46] H.-W. Hu, Y.-X. Zhang, and L. I, Multiscale cooperative microexcitations and structural rearrangements in cold dusty plasma liquids, Rev. Mod. Plasma Phys. **5**, 13 (2021).
[47] H.-W. Hu, Y.-C. Zhao, and L. I, Avalanche structural rearrangements in cold dusty plasma liquids through cascaded coherent excitations of heterogeneous multiscale thermal acoustic waves, Phys. Rev. Res. **4**, 023116 (2022).
[48] Y. Feng, J. Goree, and B. Liu, Evolution of shear-induced melting in a dusty plasma, Phys. Rev. Lett. **104**, 165003 (2010).
[49] V. Nosenko, S. Zhdanov, and G. Morfill, Supersonic dislocations observed in a plasma crystal, Phys. Rev. Lett. **99**, 025002 (2007).
[50] V. Nosenko, A. V. Ivlev, and G. E. Morfill, Microstructure of a liquid two-dimensional dusty plasma under shear, Phys. Rev. Lett. **108**, 135005 (2012).
[51] S. Plimpton, Fast parallel algorithms for short-range molecular dynamics, J. Comput. Phys. **117**, 1 (1995).
[52] See Supplemental Material at http://link.aps.org/supplemental/10.1103/PhysRevResearch.6.013288 for more details about (a) numerical method, (b) more detailed structural configurations and order parameter variations at different temperatures, (c) more examples of DC evolutions through cooperative motion-induced single bond-breaking replacements, and (d) examples of local bond-orientational order evolutions in the hexatic and the cold liquid phases.